pH sensing in aqueous solutions using a MnO2 thin film electrodeposited on a glassy carbon electrode

Nabila Cherchour, Claude Deslouis, Bouzid Messaoudi, Alain Pailleret

pH sensing in aqueous solutions using a MnO_2 thin film electrodeposited on a glassy carbon electrode

N. Cherchour[1,2,3], C. Deslouis[2,3], B. Messaoudi[1], A. Pailleret[2,3]

[1]*Laboratoire de Technologie des Matériaux et Génie des Procédés (LTMGP). Département de Génie des Procédés. Université A. Mira, Route de Targa Ouzemmour, 06000 Béjaia, Algeria.*

[2]*CNRS, UPR 15, Laboratoire Interfaces et Systèmes Electrochimiques, (LISE, case courrier 133), 4 Place Jussieu, F-75005, Paris, France*

[3]*UPMC Univ. Paris VI, UPR 15, Laboratoire Interfaces et Systèmes Electrochimiques, (LISE, case courrier 133), 4 Place Jussieu, F-75005, Paris, France*

Abstract

An electrodeposition method based on chronoamperometry was used to develop a highly reproducible and fast elaboration method of adherent manganese dioxide thin films on a glassy carbon electrode from aqueous solutions containing sulfuric acid and manganese sulfate. The resulting films were found to have a nanostructured character presumably due rather to birnessite (δ-MnO_2) than to γ-MnO_2, as suggested by their Raman and XRD signatures. They lead to modified electrodes that present an obvious although complex pH dependent potentiometric response. This sensor indeed showed a single slope non-Nernstian linear behaviour over the 1.5-12 pH range for increasing pH direction ("trace") whereas a Nernstian two slopes linear behaviour was observed for decreasing pH direction ("re-trace"). Preliminary EIS experiments carried out at a pH value of 1.8 seem to reveal a sensitivity mechanism based on proton insertion process at least at highly acidic pH values.

Introduction

In the research field dealing with the elaboration of competitive pH sensors, ongoing efforts are still mainly aimed at the elaboration of simultaneously smaller, cheaper and less fragile pH sensors providing stable responses. It is also important to propose fast and reproducible synthesis methods of such sensors as well as to widen their stability domain versus pH and temperature [1]. Among the numerous elaboration methods of pH sensors usually described in literature, those based on metallic oxides rely mainly on PtO_2 [1], TiO_2 [1], Ta_2O_5 [1], OsO_2 [1], SnO_2 [1], IrO_2 [1,2], RuO_2 [1,3,4], RuO_2-TiO_2 [5], ZrO_2 [6], PbO_2 [7] and Co_3O_4 [8,9]. Some authors have attributed the sensitivity of these oxides towards pH either to their ionic semi-conductivity, i.e. ionic conductivity acquired after insertion of dopants promoting oxygen vacancies, with the result of slightly non-stoechiometric chemical composition and/or to surface active hydroxyle groups [1,8]. Among them, RuO_2 and IrO_2 seem to be the most promising ones, as a consequence of their chemical stability and high electronic conductivity [4]. On the other hand, the rather tricky and expensive synthesis of such oxides limited substantially their interest for the elaboration of pH sensors [5,8]. In parallel, manganese dioxide (MnO_2) is probably one of the most studied oxides among transition metal oxides [10], due to the numerous combinations existing between its crystallographic varieties and the corresponding properties on one side and the consequently wide range of applications to which MnO_2 can be dedicated on the other side. For non-stoechiometric varieties, manganese dioxide exists under different crystallographic species among which γ- et ε- forms are the most electrochemically active ones in view of applications in the research domain of batteries [10,11]. MnO_2 is moreover a cheap material that is used since a long time as a cathode material in the batteries industry. MnO_2 was also suggested as a catalytic material for depollution of organic effluents, such as the oxidation of carbohydrates [12], decomposition of H_2O_2 [13], oxidation of phenol [14] or yet reduction of oxygen [15]. MnO_2 was already

shown to be a material sensitive to pH, due either to its electrochemical reduction mechanism involving presumably the introduction of protons and electrons in its structure [16-17] or to ion exchange mechanisms involving surface hydroxyle groups [17-19]. In any case, several authors have reported a Nernstian behaviour for MnO_2 over a wide pH range [16-22] but it was nevertheless observed that the measured response was highly dependent i) on the used MnO_2 sample and ii) on the ionic composition of aqueous media used for the pH measurements. For example, Qingwen et al. prepared a MnO_2 based pH sensor from a chemically synthesised MnO_2 (δ- and/or α-type) powder dispersed in an alcoholic suspension that they deposited over a graphite electrode and dried using an IR lamp. A response of -78.3 mV per pH unit was measured in HCl-KOH aqueous solutions over a 2 to 12 pH range [17]. In another contribution, Johnson *et al*. used a chemically synthesised MnO_2 powder that was then diluted in an electrolyte and compressed around a platinum electrode. The resulting pH sensor gave a response of – 75 mV/pH unit that was observed in NH_4Cl aqueous solutions over a 7 to 0 pH range [18]. Using MnO_2 powder (β-type) resulting from the thermal decomposition of manganese (II) nitrate and then treated in 10 N H_2SO_4 for a month, Tari *et al.* reported a two slope behaviour in NH_4Cl-HCl aqueous solutions. The slope of the E-pH graph was indeed found to be approximately -90 to -100 mV/pH unit and -60 mV/pH unit for pH ranges 2 to 7 and 7 to 9 respectively [20]. Interestingly, these same MnO_2 based pH sensors produced a linear variation of open circuit potential vs. pH with a slope of -60 mV/pH unit over the 0.5-5 pH range in a zinc chloride aqueous solution. A similar response is observed in $(C_2H_5)_4NClO_4$ solutions for pH values varying between 4 and 7 [21]. In the case of synthetic commercial MnO_2 powders (γ-type), the relations determined between open circuit potential and pH in NH_4Cl (pH 3-8), $ZnCl_2$ (pH 0-5) and $(C_2H_5)_4NClO_4$ (pH 2.5-8) electrolytic solutions showed a slope of -60 mV/pH unit whereas the use of NH_4Cl-HCl (pH

1-3) and $(C_2H_5)_4NClO_4$-$HClO_4$ (pH 1-2.5) solutions led to slopes of about -75 and -100 mV/pH unit [22].

The non-Nernstian behaviours observed in these published works were thought to be the result of the presence of soluble Mn^{2+} cations whose amount increases in the vicinity of MnO_2 as the pH decreases [20-22]. The MnO_2 samples used in these investigations clearly provide different sensitivity mechanisms to pH resulting indirectly from their synthesis method via their crystallographic variety and their own properties. To the best of our knowledge, all the E-pH responses reported in literature were obtained on MnO_2 powders. On the other hand, in the framework of other studies targeting other application domains, manganese dioxide has also been electrodeposited on various substrates such as platinum [23-28], gold [28-29], titanium [30-31], carbon nanotubes paper [32] and glassy carbon [28,33-36]. This latter is largely used as a cheap electrode material due to its excellent electronic conductivity, chemical inertia, impermeability to gazes and liquids as well as a high resistance towards corrosion. The originality of our contribution reported hereafter stands in the highly reproducible one-step elaboration of a new pH sensitive potentiometric electrode made from a thoroughly characterised nanostructured MnO_2 thin film electrodeposited on a glassy carbon electrode. The single mechanism by which the resulting electrode is sensitive to pH over a 11 units wide pH range is shown to be predominantly a cation insertion mechanism. This latter was identified using a fitting procedure of EIS experiments carried out in open circuit potential conditions.

I. Experimental part

The electrodeposition of MnO_2 was carried out using cyclic voltammetry or chronoamperometry in ambient conditions (T = 21 ± 1°C) in a usual three electrode electrochemical cell. The working, counter and reference electrodes were respectively a

glassy carbon disk (Φ = 3 mm, Carbone Lorraine, France), a platinum grid and a saturated mercurous sulfate electrode (SSE, E_{SSE} = 0.655 V vs. SHE). The electrochemical set-up also included a SP300 potentiostat (Bio-Logic, Claix, France). In order to prepare reproducible glassy carbon electrodes, these latter were polished using emery paper (grade 2400 and 4000) and then submitted to a thorough cleaning by sonication in bidistilled water for 5 minutes. The aqueous electrolytic solution used during the electrodeposition step contained monohydrated manganese (II) sulphate ($MnSO_4.H_2O$, 0.3 M, Sigma, France) and its pH was adjusted to 1.8 using concentrated sulfuric acid (Prolabo, France).

The morphology and the composition of the resulting MnO_2 thin films were investigated using a SEM-FEG coupled with Energy-dispersive X-ray spectroscopy (EDX).

Their cristallinity was characterised with X-Ray Diffractometry (XRD) experiments carried out at INSP laboratory (Univ. P. & M. Curie, Paris, France). In this purpose, thin films of MnO_2 electrochemically deposited on a GC working electrode were scrapped off so as to collect a MnO_2 powder. This operation was repeated until a sufficient amount of MnO_2 powder was collected for the need of XRD experiments.

Raman spectra were recorded with the help of a Labram equipment (Horiba-Jobin-Yvon) including a notch filter used as primary stage in order to reject the laser light. A grating with 1800 grooves mm^{-1} providing a 2 cm^{-1} resolution and a Peltier cooled CCD detector were also included in the setup. An excitation radiation corresponding to λ = 632.8 nm and produced by a HeNe laser was used during the experiments. Laser power is set at 0.01 mW using neutral density filters to prevent the samples from overheating during the measurements. Raman light is focused and collected in backscattering geometry with an Olympus confocal microscope, objective *100 ULWD.

The performances of the resulting pH sensors were evaluated by measuring their potentiometric response vs. SSE in test aqueous solutions whose pH was fixed using either

H_2SO_4 (Prolabo, France) and/or NaOH (Prolabo, France) solutions prepared with deionised water. The two following procedures were exploited under stirring at ambient temperature in the course of these tests (i) pH was brought from acidic to alkaline pH values using a strong acid (H_2SO_4) - strong base (NaOH) titration, leading then to the so-called "trace" on the resulting E-pH graph; (ii) pH was brought from alkaline to acidic values using the backwards titration, which then produced the so-called "re-trace" on the E-pH graph. In order to do so, a commercial pH electrode connected to a pH meter (Cyberscan ion 510) was used so as to follow the pH of the test solution in real time. The acid (or base) addition in the test solution was carried out every 200 seconds and a 150 seconds stabilisation time was respected before the pH and potential values were read.

EIS experiments were carried out in the 100 kHz – 10 mHz frequency range by plotting spectra using ten points per frequency decade. During experiments, a platinum wire was connected in parallel with the SSE reference electrode so as to avoid well-known artefacts due to saturated reference electrodes in the high-frequency domain [37]. Theoretical impedance expression detailed further was fitted to experimental spectra using a home-made fitting software.

II. Results and discussion

1. Synthesis and structural characterisation of electrodeposited MnO_2 thin films

The anodic sweep of the first cycle of the voltammogram (see Figure 1), corresponding to electrodeposition of MnO_2 on GC, shows an oxidation peak appearing at 695 mV vs. SSE with a very sharp increase which cannot be assigned, as reported in literature, to a single electron transfer between Mn^{2+} in solution and the electrode.

In fact, the reaction leading to the formation of MnO_2 is an overall one according to [38]:

$$Mn^{2+} + 2H_2O \leftrightarrows MnO_2 + 4H^+ + 2e^- \quad (1)$$

An initial model introduced by Paul and Cartwright [39], and later confirmed by Petitpierre et al. [23] resolved this reaction in an ECE three steps mechanism:

$$Mn^{2+} \leftrightarrows Mn^{3+} + e^- \quad (2)$$

$$Mn^{3+} + 2\,H_2O \leftrightarrows MnOOH + 3H^+ \quad (3)$$

$$MnOOH \leftrightarrows MnO_2 + H^+ + e^- \quad (4)$$

These reactions were originally written as irreversible reactions, but as in further works, forward and/or backward reactions or some of their combinations were considered, they are therefore presented here as reversible ones though they imply different phases.

In reference [39], the voltammograms obtained over wide Mn^{2+} concentration and pH domains allowed to point up easily the first step (reaction (2)) at very acidic pH. For increasing pH, they display the same aspect as in Figure 1. The considered synthesis pH (1.8) is not sufficiently acidic to avoid the formation of MnOOH according to equation (3). Then, due to the very low solubility product, one may assume that as soon as Mn^{3+} is formed with a detectable concentration at the interface, MnOOH precipitates and forms an insulating thin film, through which Mn^{2+} diffusion is strongly slowed down and therefore the current keeps a negligible value. Both γ-MnOOH (manganite) and β-MnOOH (feitknechtite) have been also observed as initial oxygenation products. MnOOH phases are sparingly soluble in the absence of strongly complexing ligands, or unless pH is very low. According to [40], the aqueous concentration of $[Mn^{3+}]$ in equilibrium with γ-MnOOH would be approximately 10^{-21} M at pH 7 and 25°C, the solubility product, K_{s0}, being approximately 10^{-42}.Once the potential reaches a value at which forward reaction (4) becomes quantitative, MnOOH is fastly transformed into MnO_2 which has sufficient electronic conductivity to ensure current at its

surface corresponding to forward reaction (2). MnOOH appears then as a minor intermediate which does not limit the current. One should also point out that at this potential (695 mV vs. SSE which is close to 1.1 V vs. SCE), O_2 evolution may proceed and produce direct oxidation of Mn^{2+} at the electrode according to:

$$Mn^{2+} + 1/4\ O_2 + 3/2\ H_20 \rightarrow MnOOH + 2\ H^+ \quad (5)$$

This scenario can explain the sharp current increase at 695 mV vs. SSE.

In the reverse cathodic sweep, two cathodic peaks are observed at +406 and -194 mV vs. SSE (see Figure 1). The less cathodic one was assigned to the MnO_2 reduction (backward reaction (4) and the other one to direct reduction of MnOOH into Mn^{2+} (combination of backward reactions (3) and (2)) [25, 26, 29] :

When pH domain becomes more acidic, MnOOH becomes unstable and disproportionation may occur :

$$2\ MnOOH + 2\ H^+ \rightarrow MnO_2 + Mn^{2+} + 2\ H_2O \quad (6)$$

The global reduction can then be written as the backward reaction (1).

In the presence of Mn^{2+}, backward reactions (3) and (6) may also proceed together with [23-25, 29]:

$$MnO_2 + Mn^{2+} + 4\ H^+ \rightarrow 2\ Mn^{3+} + 2\ H_2O \quad (7)$$

Mn^{3+} ions thus generated can then be electrochemically reduced to Mn^{2+} according to backward reaction (2).

Among the various electrochemical techniques allowing the electrodeposition of very adherent MnO_2 thin films, chronoamperometry was chosen preferentially for its easy and quick use. A chronoamperogram corresponding to a 695 mV vs. SSE electrodeposition potential (which is the value measured for the anodic peak potential in Figure 1) is shown in

Figure 2a. After a sharp peak followed by a fast drop corresponding to double layer charging and simultaneous nucleation/growth process of the manganese dioxide thin film, the current reaches a non zero steady value with an extremely slow kinetics (about two hours duration). The current has been plotted as a function of the reciprocal of the square root of time: it does not show a single straight line. As a consequence, the current measured does not strictly follow the Cottrell equation, as expected in the case of a semi-linear infinite diffusion. However, if one excludes the first four points ($t < 4$ s) due to both uncertainty on zero time and on influence of ohmic drop and charge transfer resistances, one observes roughly two linear domains with a cut-off around $t \sim 10^2$ s. Then those two domains could reflect for $t < 10^2$ s, diffusion in the liquid phase corresponding to Mn^{2+} diffusion towards the electrode (no stirring) and the second domain ($t > 10^2$ s), diffusion of Mn^{3+} in MnOOH phase, the final steady current being governed by MnO_2 growth rate.

The thickness of the electrodeposited MnO_2 was calculated using Faraday's law by considering that the film is compact:

$$d = \frac{Q.M_{MnO_2}}{z.F.s.\rho} \qquad (8)$$

In this equation, d is the thickness of the film, Q, the coulombic charge measured below the chronoamperogram (see Figure 2), M_{MnO2}, the molar mass (86.94 g/mol) and ρ, the density (5.026 g/cm^3 [41]) for manganese dioxide, F, the Faraday's constant (96485 C/mol), s, the area of the GC working electrode (0.07 cm^2), and z, the number of electrons exchanged in the redox reaction (2 here). These calculations led to thicknesses varying between 93 nm and 542 nm for electrodeposition times varying between 30 s and 300 s. The influence of the deposition potential on the MnO_2 film thickness was also investigated using potential values either lower or higher than the anodic peak potential (695 mV vs. SSE) using a 60 s deposition time (see Figure 3). The other deposition parameters (composition of the electrolytic solution, electrodeposition technique, temperature…) were the same as those

reported for Figures 1 and 2. Up to five depositions were carried out for each potential value so as to check for the reproducibility of consumed electrical charges and subsequent calculated thicknesses. The thickness of the resulting films was found to increase from 40 nm up to 160 nm as the deposition potential varied from 625 to 695 mV vs. SSE. Beyond this second value, the film thickness is stable and then slightly decreases as the deposition potential increases to reach 1086 mV vs. SSE, a potential at which oxygen production starts occurring.

The electrodeposited MnO_2 films were first characterised using SEM-FEG. Whether the electrochemical technique used for their production was chronoamperometry or cyclic voltammetry, SEM-FEG images showed porous films made of sets of randomly oriented nanometric needles (see Figure 4a). As a consequence of this porosity, it is likely that the thicknesses values calculated from Eq. (7) were underestimated. For deposition times longer than 30 seconds, cracks frequently appeared on these MnO_2 films prior to or during SEM-FEG observations and presumably as a consequence of the drying step in air. This led us to use only MnO_2 thin films resulting from 30 seconds chronoamperometric deposition procedures to carry out our pH sensing investigations. EDS analysis revealed the presence of oxygen and manganese in these films with the expected 2:1 ratio for manganese dioxide (see Figure 4b).

The Raman spectrum shown in Figure 5 displays four rather well-defined Raman bands appearing respectively at 510 , 574 , 649 and 731 cm^{-1} respectively as well as a fifth broader one at 294 cm^{-1}. The 574 and 649 cm^{-1} bands are clearly dominating the spectrum. These Raman shift values allowed us to rule out the α- and β- varieties of manganese dioxide [42,43] as well as γ-MnOOH [43]. They better correspond to those observed for γ-MnO_2, a cristallographic variety known to result from a random intergrowth of pyrolusite layers in a ramsdellite matrix [10,44]. Let us nevertheless notice that the band at 294 cm^{-1} was shown to

appear only in the Raman spectrum of pure ramsdellite and not in that of γ-MnO_2. In parallel, bands appearing at 649 cm^{-1} in our spectrum can only be attributed to γ-MnO_2 characterised by a rather high rate of pyrolusite intergrowth (P_r) indicating the fraction of single chain slabs in a given double chain (ramsdellite) framework. At this stage, one can only suggest that our MnO_2 thin films may be constituted of pure ramsdellite mixed with γ-MnO_2. Nevertheless, a close comparison of the Raman shifts identified in our spectrum with those reported for sol-gel birnessite reveals striking similarities, which makes birnessite (δ-MnO_2) another possible variety for our manganese dioxide thin films [45]. In any case, a basic conclusion is that the obtained thin film is a manganese dioxide, and preferably birnessite or a mixture of γ-MnO_2 with ramsdellite.

The XRD spectrum shown in Figure 6 displays seven peaks. The most intense peak situated at $2\theta = 11.755$ seems to be sufficient to rule out γ- crystallographic variety of MnO_2 even though the other six peaks observed in Figure 6 could reasonably be attributed to γ-MnO_2 (see sample 6 in appendix 1 of [10]. This intense peak as well the others appearing in our XRD spectrum suggest that our films rather belong to the birnessite, or δ-type crystallographic variety [46-48].

2. Potentiometric response of a GC/MnO_2 based pH sensor

The potentiometric response of an electrode resulting from the electrodeposition of a MnO_2 thin film on GC electrode is shown as a function of time (see Figures 7a, 8a and 8b) and pH (see Figures 7b and 8c) in open circuit conditions. Over the duration of the experiment plotted in Figure 7 (approximately 11 000 sec., or a bit more than three hours), the solution pH varies initially from 1.04 to 6 (“trace”) as a consequence of the addition of small volumes of an aqueous NaOH solution to an aqueous solution containing initially sulphuric acid only, and then from 6 to 1.04 (“re-trace”) with the help of further additions of small volumes of an aqueous H_2SO_4 solution. Trace and re-trace shown in Figure 7b both indicate a linear relation

between potential and pH over the investigated pH range. The sensitivity of the GC/MnO_2 sensor is approximately the same in both cases as shown by the two slopes (97.7 mV/pH unit on trace and 101.5 mV/pH unit on re-trace) measured respectively on trace and re-trace in Figure 7, in spite of a 20 mV shift existing between them.

Observations are substantially different when the investigated pH range is extended to 12 (see Figure 8). Over the duration of the experiment plotted in Figure 8 (approximately 25 000 sec., or a bit less than 7 hours), the solution pH varies initially from 1.5 to 12 (trace) with the help of NaOH additions to an aqueous solution containing initially sulphuric acid only, and then from 12 to 1.5 (re-trace) using additions of small volumes of an aqueous H_2SO_4 solution. The trace can be considered as a single linear variation of potential as a function of pH (see Figure 8c), in spite of a deviation from linearity between 6.5 and 9 indicating an instability domain of our sensor in this pH range, whereas the re-trace is clearly made of two linear parts (see Figure 8c). The trace indeed shows a linear but non-Nernstian behaviour (slope was -87.7 mV/pH unit (in Figure 8c) with a correlation coefficient of 0.998. The slope of the E-pH graph corresponding to the trace was found to vary between -84 mV/pH unit and -97 mV/pH unit with an average value of -92 ± 5.2 mV/pH unit.

As far as the two slopes behaviour observed on the re-trace is concerned, the values of the slopes are -57.7 mV/pH unit for pH values varying between 12 and 6 (correlation coefficient: 0.999), and -122.3 mV/pH unit when the pH varies from 6 to 1.5 (correlation coefficient: 0.999). More precisely, the slope related to variation law observed between 6 and 1.5 on the re-trace varies between -122.3 and -143.2 mV/pH, with an average value of -134.3 ± 6.3 mV/pH unit, whereas the one observed between 12 and 6 on the re-trace varies between -57.7 and -73.5 mV/pH unit, with an average value of -67.7 ± 3.8 mV/pH unit.

It must be emphasised here that trace and re-trace data were obtained in separate runs each with freshly prepared MnO_2 thin films using fresh initial solutions whose pH were 1.5 and 12

respectively. Other tests carried out in identical experimental conditions presented a very satisfying reproducibility. The relations shown in Figure 8 between the open circuit potential and the pH were systematically observed, whether the experiments corresponding to the trace and the re-trace were carried with a single or with two different MnO_2 films, using either a single or two different aqueous solutions, and whether the trace was plotted before or after the re-trace. This important fact suggests therefore that the feature observed for $7 < pH < 9$ in Figure 8 is neither a consequence of the ionic strength, nor of the aging or the dissolution of the MnO_2 film.

Interestingly, Figures 7 and 8 show consecutive pH measurements over approximately 11 000 sec. (or a bit more than three hours) and 25 000 sec. (or a bit less than 7 hours) respectively. As our MnO_2 film is not prone to aging, it is therefore established from Figures 7 and 8 that it can be used for consecutive pH measurements for more than seven hours without any alteration of its response. One can remind as well that this sensor can be easily renewed by a fast chronoamperometric electrodeposition of a brand new MnO_2 thin film.

During these pH sensing tests using a GC/MnO_2 electrode, manganese dioxide may react with protons according to reaction (7). In this case, the equilibrium potential (or open circuit potential) is $E_{MnO2/MnOOH}$ and it can be expressed with the help of the Nernst expression for this redox couple:

$$E_{MnO2/MnOOH} \text{ vs. NHE} = E^0_{MnO2/MnOOH} \text{ vs. NHE} - 0.059\ pH \qquad (9)$$

According to the table of standard potentials (given at 25°C), $E^0_{MnO2/MnOOH} = 1.16$ V vs. NHE = 0.505 V vs. SSE, which leads for Equation (9) to:

$$E_{MnO2/MnOOH} \text{ vs. SSE} = 0.505 - 0.059\ pH \qquad (10)$$

MnO_2 may also react with four protons following reaction (1). The corresponding equilibrium potential would then be expressed as $E_{MnO2/Mn^{2+}}$:

$$E_{MnO2/Mn}^{2+} \text{ vs. NHE} = E^{0}_{MnO2/Mn}^{2+} \text{ vs. NHE} - 0.118\ pH - 0.03 \log[Mn^{2+}] \quad (11)$$

with $E^{0}_{MnO2/Mn}^{2+} = 1.23$ V vs. NHE = 0.575 V vs. SSE.

As a consequence, Equation (11) becomes:

$$E_{MnO2/Mn}^{2+} \text{ vs. SSE} = 0.575 - 0.118\ pH - 0.03 \log[Mn^{2+}] \quad (12)$$

By comparison between Equations (10) and (12) on one side, and the slope values observed experimentally for the trace on the other side, one can conclude that these latter are different from the slope of 118 mV/pH unit expected from reaction (1) (see expression 12) but rather comparable to those reported by Tari and Hirai [20-22]. These authors suggest that the difference between the experimental and theoretical values results from the amount of dissolved Mn^{2+} cations that is expected to increase as the pH decreases. This constituted a confirmation of results reported by Kozawa [49] where a -90 mV/pH unit slope was observed as a consequence of the release of soluble Mn^{2+} cations produced by reaction (1). These Mn^{2+} cations may then react with MnO_2 at the MnO_2/electrolytic solution interface according to reaction (7), which may substantially alter the potential-pH response of our GC/MnO_2 based pH sensor.

As far as the re-trace (titration of the alkaline solution with sulfuric acid) is concerned, two linear variations can be clearly identified in Figure 8c. The slope values given above are very close to the theoretical values of -59 mV/pH unit and -118 mV/pH unit appearing in Equations (10) and (12) respectively and corresponding respectively to reactions (6) and (1). Let us notice that the change of slope appears at pH 6, which is inside the range of values usually suggested in literature for the isoelectric point of manganese dioxides [50]. These observations are quite similar to those reported in literature [51-52], confirming thus that the behaviour of this GC/MnO_2 based pH sensor is not the same for the trace and the re-trace, and therefore depends on the way the pH range is described. This observation was further strengthened by the fact that the one- or two-slope variation illustrated in Figure 8c were

always observed, whether the trace and re-trace were obtained with only one MnO_2 film and only one aqueous solution, one MnO_2 film for the trace and another one for the re-trace and still only one aqueous solution, or yet one MnO_2 film for both the trace and the re-trace and one aqueous solution for the trace and another one for the re-trace. Moreover, the slopes measured for the three linear variation laws were always found to be close to those reported above within a ± 5 mV range in our experimental conditions.

3. EIS measurements

In order to develop a better understanding of the processes ruling the complex sensitivity mechanism of our sensor towards pH, preliminary EIS experiments were carried out in open circuit conditions in an acidic aqueous solution (pH 1.8) corresponding to synthesis conditions either at a bare or MnO_2 coated GC electrode. Resulting spectra are shown in Figure 9.

The EIS spectrum relative to bare GC electrode (Figure 9a) shows two linear domains in the HF and Mid Frequency (MF) ranges. The slope is lower in the HF range (about 55°). Though this behaviour looks similar to that displayed by a porous electrode idealized as a set of adjoining cylindrical pores, the rather higher slope than 45° for the latter case, motivated us to consider an intermediate geometry between flat (slope 90° for purely capacitive) and adjoining pores (slope 45° for purely capacitive).

The EIS spectrum on GC/MnO_2 electrode shows a flattened semi-circle in the HF range followed by a linear domain in the MF range of slope around 35°. For both electrodes (GC and GC/MnO_2), the LF range indicates a capacitive-like behaviour, but rather characterised by a Constant Phase Element (CPE) with a limit angle lower than 90°.

The two electrodes behave thus as ideally polarisable electrodes without Faradaïc current. In the case of GC/MnO_2 electrode, the aspect of the HF and MF ranges led us to assign the frequency dependence to an insertion process. As the solution was free from Mn species, the only transient electron transfer occurring at the GC/MnO_2 interface was attributed to reaction

(4). This was balanced by the insertion-removal of protons at the film solution interface given by the same reaction (Scheme in Figure 10).

Therefore spectra for both electrodes have been analysed with the help of impedance model corresponding to an electrode with non adjoining pores reported in scheme of Figure 11: MnO_2 film appears to be thin enough so that the original porosity of the substrate is preserved in the GC/MnO_2 electrode.

According to scheme in Figure 11, the surface is distributed between pores (n pores of radius r per unit area,) and the complementary flat surface of area ($1 - n\pi r^2$).

Within a pore, it has been established earlier [53-54] that, in the absence of concentration distribution of electroactive species, the impedance corresponding to the transmission line figured in Figure 11 is given by:

$$Z_{p1} = \sqrt{R_{01}Z_{01}}\coth\left\{\ell\sqrt{\frac{R_{01}}{Z_{01}}}\right\} \qquad (13)$$

Where, ℓ is the pore depth, R_{01} is the ohmic drop within one pore of unit length (1 cm), Z_{01} is the interfacial impedance at the oxide-solution interface corresponding to the lateral area of a pore of unit length.

One has also:

$$R_{01} = \frac{\rho}{\pi r^2} \text{ where } \rho \text{ is the solution resistivity } (\Omega.\text{cm}). \qquad (14)$$

If Z represents the interfacial impedance per unit area, then one has;

$$Z_{01} = \frac{Z}{2\pi r} \qquad (15)$$

If one deals with non adjoining pores, the experimental impedance is defined as:

$$Ze = R_s + \frac{1}{\frac{n}{Z_{p1}} + \frac{1 - n\pi r^2}{Z}} \qquad (16)$$

R_s is the ohmic drop of the electrolyte and the High Frequency (HF) limit of the diagram.

R_s is a fitted parameter. For an RDE electrode, its value is related to the solution resistivity from Newman's equation [55] as:

$$R_s = \frac{\rho}{4R} \tag{17}$$

Where R is the disc radius. The used substrate was a glassy carbon rod (r = 0.15 cm).

As R_{01} and R_s are among the fitted parameters, one can define the pore radius r as:

$$r = \sqrt{\frac{0.6R_s}{\pi R_{01}}} \tag{18}$$

The interfacial impedance then as to be calculated.

(i) In the simplest case for a blocking electrode, Z_{01} is a double layer capacitance. This is the case of bare glassy carbon. Here Z_{01} was taken as a CPE (Figure 11)

(ii) As said above, the case of GC/MnO_2 electrode was considered analogous to an insertion process. Such an insertion process has been earlier represented by the electrical equivalent circuit displayed in Figure 11c and proposed for the doping process of a conducting polymer [56]. In this equivalent circuit, $R_{GC/MnO2}$ is the charge transfer resistance corresponding to the electron exchange at the metal-oxide interface; $C_{GC/MnO2}$ mox is the associated space charge capacitance. $R_{MnO2/sol}$ is the charge transfer resistance corresponding to the ion (H^+) exchange at the oxide-solution interface and $C_{MnO2/sol}$ the associated space charge capacitance. W is the linear restricted diffusion (LRD) impedance corresponding to the fact that H^+ flux is zero value at the metal-oxide interface [57].

$$W = Rd\frac{\coth(j\omega\tau)^{1/2}}{(j\omega\tau)^{1/2}} \quad (19)$$

$\omega/2\pi$ is the frequency (Hz) and τ is the time constant associated to H^+ diffusion in the oxide. Rd is the diffusion resistance. In the LF range, when there is no faradaïc current, the behaviour is purely capacitive and given by this specific diffusion term characterizing insertion. Considering also that the low frequency behaviour is never purely capacitive but rather shows CPE behaviour, Warburg impedance is better expressed as "modified" LRD:

$$W = Rd\frac{\coth(j\omega\tau)^{\alpha/2}}{(j\omega\tau)^{\alpha/2}} \quad (20)$$

Where α is a CPE exponent, with $0 < \alpha < 1$ but in general close to 1.

The use of this impedance model based on an insertion phenomena occurring in a supposedly dense manganese dioxide electrodeposited on a glassy carbon electrode presenting non-adjoining pores allows fitting very efficiently the EIS spectra shown in Figure 9. The set of fitted parameters is reported in Table 1.

Further experiments are currently underway to confirm this model all over the investigated pH range so as to better view the trends in the parameters evolution with pH and get a better estimate of the confidence intervals on parameters. At the present stage of our investigations, one can reasonably suggest that the sensitivity mechanism of our GC/MnO_2 in highly acidic solutions is based on an insertion mechanism of protons in the manganese dioxide matrix.

Conclusion

Nanostructured manganese dioxide thin films can be electrodeposited on a glassy carbon electrode in a highly reproducible and fast manner by employing chronoamperometry with a 695 mV/SSE potential during 30 sec in an aqueous solution containing manganese sulfate (0.3 M) and sulfuric acid (pH=1.8) at 21°C. The resulting modified electrode was shown to be a

potentiometric pH sensor over the pH range situated between 1 and 12 even though its response was found to be dependent on the variation direction of the pH. This sensor indeed showed a single slope non-Nernstian linear behaviour over the whole pH range as this latter increased from 1.5 to 12 (trace) whereas a Nernstian two slopes linear behaviour is observed when pH decreased from 12 to 1.5 (re-trace). This peculiar behaviour was observed whether the trace and the re-trace were obtained both or each with a single manganese dioxide thin film, with a single aqueous solution having the adequate pH, whatever the pH of the starting point was (1.5 or 12). Preliminary EIS experiments carried out at a pH value of 1.8 seem to reveal a sensitivity mechanism based on proton insertion process at least at highly acidic pH values.

Acknowledgements

Warm acknowledgements are addressed to M.C. Bernard for her contribution during Raman spectroscopy experiments, to S. Borensztajn (LISE), F. Pillier (LISE) and S. Hidki (INSP, UPMC) for their expertise and experimental support in SEM-FEG/EDX and XRD experiments respectively, to P. Rousseau for the development of the fitting software used in this work and finally to V. Vivier for fruitful discussions respectively. N. Cherchour warmly acknowledges Egide for a financial support in the frame of a PHC-Tassili type program (N° 06MDU686) as well as the Algerian government and CNOUS (France) for a PROFAS type financial support.

Bibliography

[1] A. Fog, R.P. Buck, Sens. Actuators, B 5 (1984) 137-146.

[2] J. Hendrikse, W. Olthuis, P. Bergveld, Sens. Actuators, B 53 (1998) 97-103.

[3] Y. H. Liao, J.C. Chou, Sens. Actuators, B 128 (2008) 603-612.

[4] H.N. McMurray, P. Douglas, D. Abbot, Sens. Actuators, B 28 (1995) 9-15.

[5] L.A. Pocrifka, C. Gonçalves, P. Grossi, P.C Colpa, E.C. Pereira, Sens. Actuators, B 113 (2006) 1012-1016.

[6] S. Ardizzone, M. Radaelli, J. Electroanal. Chem., 269 (1989) 461-469.

[7] A. Elfakhari, Sens. Actuators, B 88 (2003) 234-238.

[8] L. Qingwen, L. Guoan, S. Youqin, Anal. Chim. Acta, 109 (2000) 137-142.

[9] R. Garavaglia, C.M. Mari and S. Trasatti, Surf. Tech., 23 (1984) 41-47.

[10] Y. Chabre, J. Pannetier, Prog. Solid State Chem. 23 (1995) 1-130.

[11] C-H. Kim, Z. Akase, L. Zhang, A.H. Heuer, A.E. Newman, P. Hughes, J. Solid State Chem., 179 (2006) 753-775.

[12] D. Das, P.K. Sen, K. Das, Electrochim. Acta, 54 (2008) 289-295.

[13] W. Zhang, H. Wang, Z. Yang, F. Wang, Colloids Surf., A, 304 (2007) 60-66.

[14] Y. Dong, H.X. Yang, K. He, S. Song, A. Zhang, Appl. Cat., B, 85 (2009) 155-161.

[15] B. Klapste, J. Vondrak, J. Velicka, Electrochim. Acta, 47 (2002) 2365-2369.

[16] A. Kozawa, J.F. Yeager, J. Electrochem. Soc., 112(10), (1965), 959-963.

[17] L. Qingwen, W. Yiming, L. Guoan, Sens. Actuators B 59 (1999) 42-47.

[18] R.S. Johnson, W.C. Vosburgh, J. Electrochem. Soc, 99 (1952) 317-322.

[19] A. Kozawa, J. Electrochem. Soc., 106(7) (1959) 552-556.

[20] I. Tari, T. Hirai, Electrochim. Acta, 26 (1981) 1657-1660.

[21] I. Tari, T. Hirai, Electrochim. Acta, 27 (1982) 149-152.

[22] I. Tari, T. Hirai, Electrochim. Acta, 27 (1982) 235-238.

[23] J.Ph. Petitpierre, Ch. Comninellis, E. Plattner, Electrochim. Acta, 35 (1990) 281-287.

[24] S. Bordoardo, J. Brenet, M. Maja, S. Spinelli, Electrochim. Acta, 39 (1994) 1999-2004.

[25] S. Nijjer, J. Thonstad, G.M. Haarberg, Electrochim. Acta, 46 (2000) 395-399.

[26] S. Rodrigues, N. Munichandraiah, A. Shukla, J. Appl. Electrochem., 28 (1998) 1235-1241.

[27] H.Y. Lin, Y.P. Sun, B.J. Weng, C.T. Yang, N.T. Suen, K.H. Liao, Y.C. Huang, J.Y. Ho, N.S. Chong, H.Y. Tang, Electrochim. Acta, 52 (2007) 6548-6553.

[28] W.C. Maskell, J. Electroanal. Chem., 198 (1985) 127-137.

[29] Z. Rogulski, H. Siwek, I. Paleska, A. Czerwinski, J. Electroanal. Chem., 543 (2003) 175-185.

[30] S. Nijjer, J. Thonstad, G.M. Haarberg, Electrochim. Acta, 46 (2001) 3503-3508.

[31] E. Preisler, J. Appl. Electrochem., 19 (1989) 559-565.

[32] S.L. Chou, J.Z. Wang, S.Y. Chew, H.K. Liu, S.X. Dou, Electrochem. Commun., 10 (2008) 1724-1727.

[33] J. Di, F. Zhang, Talanta, 60 (2003) 31-36.

[34] Z. Rogulski, A. Czerwinski, J. Power Sources, 114 (2003) 176-179.

[35] A. Manivel, N. Ilayaraja, D. Velayutham, M. Noel, Electrochim. Acta, 52 (2007) 7841-7848.

[36] J.A. Lee, W.C. Maskell, F.L. Tye, J. Electroanal. Chem., 79 (1977) 79-104.

[37] A.-T. Tran, F. Huet, K. Ngo, P. Rousseau, Electrochim. Acta, 55 (2010) 1645-1655.

[38] A. Kozawa, in "Batteries Vol.1 Manganese Dioxide" edited by K.V. Kordesch, Marcel Dekker, New York, 1974.

[39] R.L. Paul, A. Cartwright, J. Electroanal. Chem., 201 (1986) 113-122.

[40] J.K. Klewicki and J.J. Morgan, *Environ. Sci. Technol.* **32** (1998), pp. 2916–2922

[41] Toxicological sheet N°52, INRS, 1997.

[42] Q. Tang, X. Huang, C. Wu, P. Zhao, Y. Chen, Y. Yang, J. Mol. Catal. A: Chem., 306 (2009) 48-53.

[43] T. Gao, H. Fjellvåg, P. Norby, Anal. Chim. Acta, 648 (2009) 235-239.

[44] C. Julien, M. Massot, S. Rangan, M. Lemal, D. Guyomard, J. Raman Spectrosc., 33 (2002) 223-228.

[45] C. Julien, M. Massot, R. Baddour-Hadjean, S. Franger, S. Bach, J.P. Pereira-Ramos, Solid State Ionics, 159 (2003) 345-356.

[46] D. Portehault, S. Cassaignon, E. Baudrin, J.-P. Jolivet, J. Mater. Chem., 19 (2009) 2407-2416.

[47] V.A. Drits, E. Silvester, A.I. Gorshkov, A. Manceau, Am. Mineral., 82 (1997) 946-961.

[48] S. Devaraj, N. Munichandraiah, J. Solid State Electrochem., 8 (2005) A373-A377.

[49] A. Kozawa, Extended Abstract, Vol. 75-2, p.24, U. S. Electrochem. Soc. (1975).

[50] B. Prélot, C. Poinsignon, F. Thomas, E. Schouller, F. Villéras, J. Colloid Interf. Sci. 257 (2003) 77-84.

[51] H.F. McMurdie, D.N. Craig, G.W. Vinal, Trans. Electrochem. Soc., Vol. 90 (1946) 449-465.

[52] C. Drotschmann, Metall, 37 (1948).

[53] R. de Levie, in "Advances in Electrochemistry and Electrochemical Engineering" (Ed. By P. Delahay), Vol. VI, p. 329, Interscience, John Wiley and Son, New York (1967).

[54] J.P. Candy, P. Fouilloux, M. Keddam and H. Takenouti, Electrochim. Acta, 26 (1981) 1029.

[55] J.S. Newman, *Electrochemical Systems*; Prentice Hall: Englewodd Cliffs, New Jersey, USA, 1991.

[56] H. Nguyen Thi Le, B. Garcia, Q. Le Xuan, C. Deslouis, Electrochim. Acta, 46, (2001) 4259.

[57] J.S. Chen, J.-P. Diard, R. Durand, C. Montella, J. Electroanal. Chem., 406 (1996) 1.

Table(s)

	Rs Ω	Pore radius nm	Pores number cm^{-2}	τ s	α	$R_{GC/MnO2}$ Ω cm^2	$R_{MnO2/sol}$ Ω cm^2	$C_{GC/MnO2}$ μF cm^{-2}	$C_{MnO2/sol}$ μF cm^{-2}	Rd Ω cm^2
GC	181	274	$2.1\ 10^6$							
GC/MnO_2	93.5	267	$2.4\ 10^6$	1	0.44	12.7	65.5	1.1	1.05	2320

Table 1: Fitted parameters values corresponding to elements of Figure 11.

Figure(s)

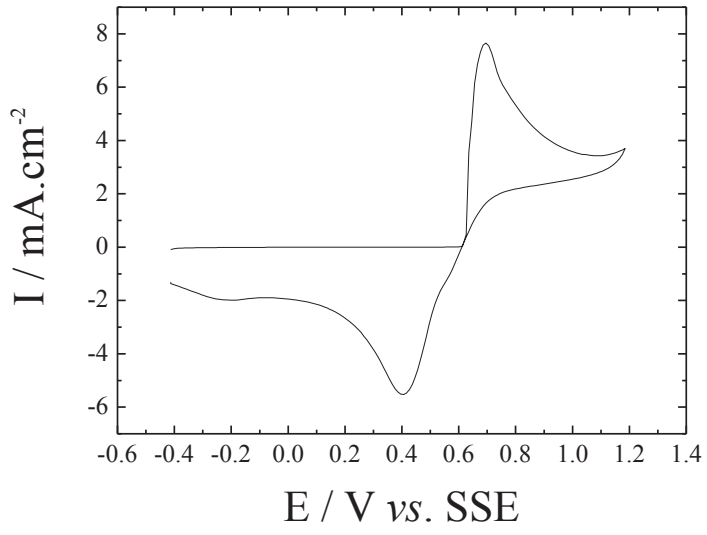

Figure 1: Cyclic voltammogram obtained on a glassy carbon electrode (s = 0.07 cm^2) in an aqueous electrolytic solution containing $MnSO_4.H_2O$ (0.3 M) and H_2SO_4 (pH 1.8). Scan rate: 10 mV/s. T : 21 °C.

Figure(s)

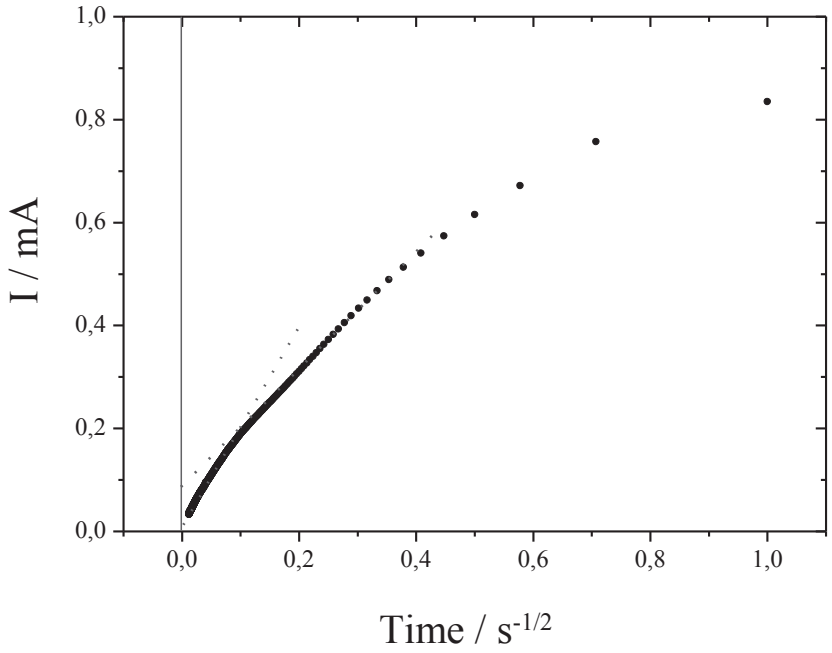

Figure 2: Graph I = $f(t^{-1/2})$ plotted with the help of the data of a chronoamperogram corresponding to the electrodeposition of a MnO_2 thin film on glassy carbon (s = 0.07 cm^2). $E_{appl.}$= 0.695 V vs. SSE in an aqueous electrolytic solution containing $MnSO_4.H_2O$ (0.3 M) and H_2SO_4 (pH = 1.8). Deposition time : 2 h. T : 25 °C.

Figure(s)

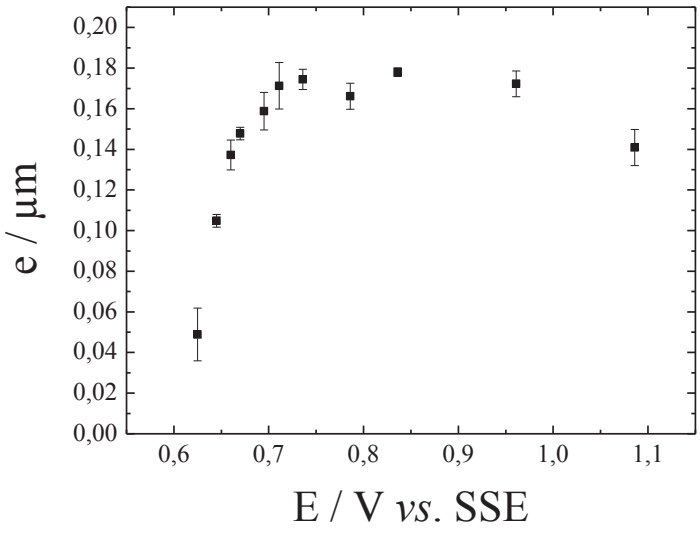

Figure 3: Graph showing the variation of the thickness (calculated from Faraday's law considering a perfectly dense MnO_2 film) as a function of the deposition potential. The electrolytic solution used for the deposition is the same as the one reported for Figures 1 and 2. Deposition time : 60 s. T : 21 °C.

Figure(s)

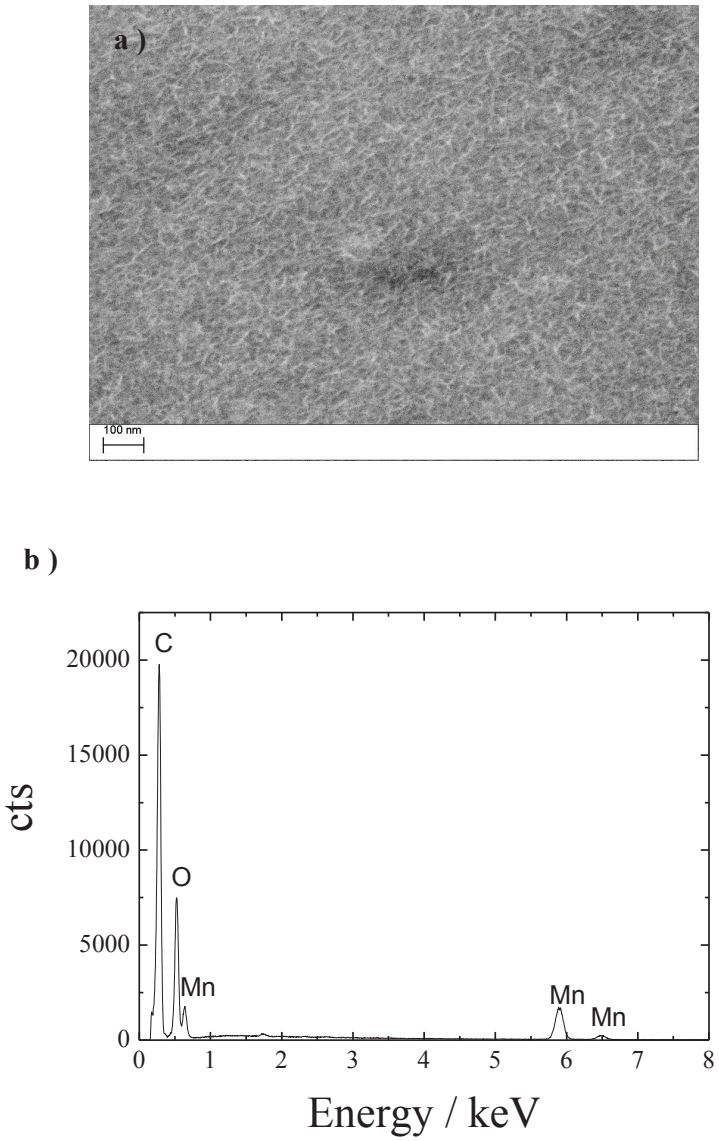

Figure 4: a) SEM-FEG image and b) EDS analysis of a MnO_2 thin film electrodeposited using chronoamperometry on a GC electrode (s = 0.07cm^2) in an aqueous electrolytic solution containing $MnSO_4.H_2O$ (0.3 M) and H_2SO_4 (pH = 1.8). $E_{appl.}$ = 0.695 V vs. SSE. Deposition time : 30 s. T : 21 °C.

Figure(s)

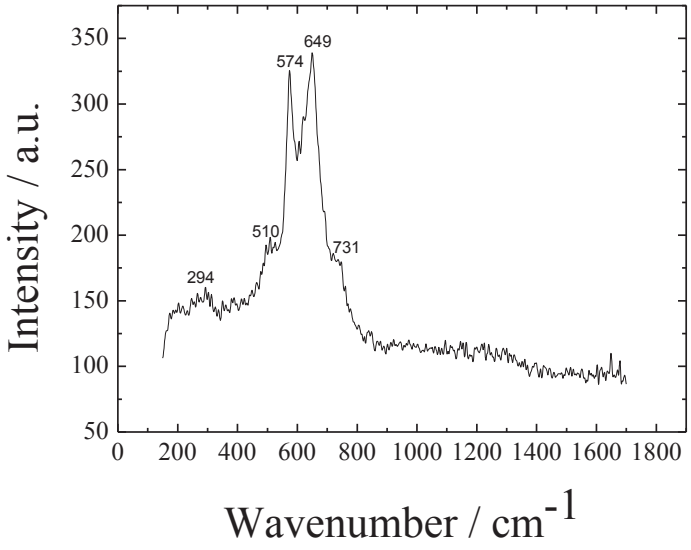

Figure 5: Raman spectrum of a MnO_2 thin film electrodeposited using chronoamperometry on a GC electrode (s = 0.07 cm^2) in an aqueous electrolytic solution containing $MnSO_4.H_2O$ (0.3 M) and H_2SO_4 (pH = 1.8). $E_{appl.}$ = 0.695 V vs. SSE. Deposition time : 5 min. T : 21 °C.

Figure(s)

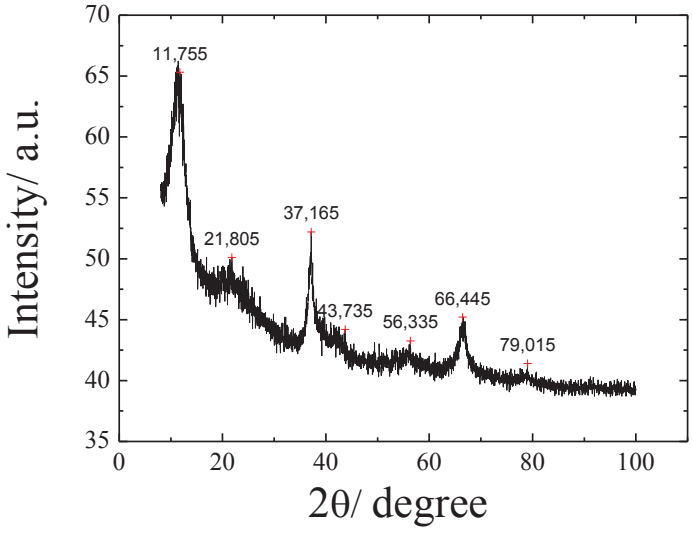

Figure 6: XRD spectrum of a MnO_2 powder produced by scratching a GC electrode (s = $0.07cm^2$) on which the MnO_2 thin film had been initially electrodeposited using an aqueous electrolytic solution containing $MnSO_4.H_2O$ (0.3 M) and H_2SO_4 (pH=1.8). $E_{appl.}$ = 0.695 mV vs. SSE. Deposition time : 30 s. T : 21 °C.

Figure(s)

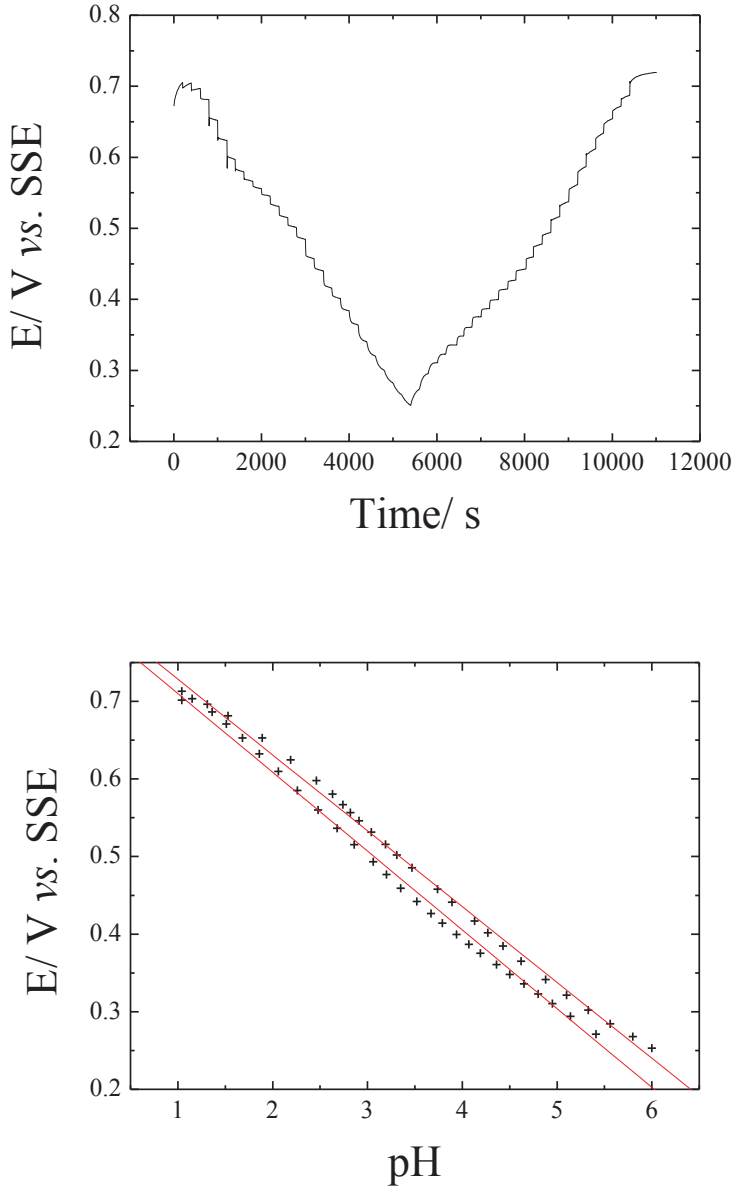

Figure 7: Potentiometric response of an electrode resulting from the electrodeposition of a MnO_2 thin film on a glassy carbon electrode : open circuit potential plotted as a function of a) time, b) pH. The investigated pH range was described as follows: 1) trace (titration of an aqueous H_2SO_4 solution with an aqueous NaOH from pH 1.04 to 6), 2) re-trace (titration of the resulting solution with an aqueous H_2SO_4 solution from pH 6 to 1.04).

Figure(s)

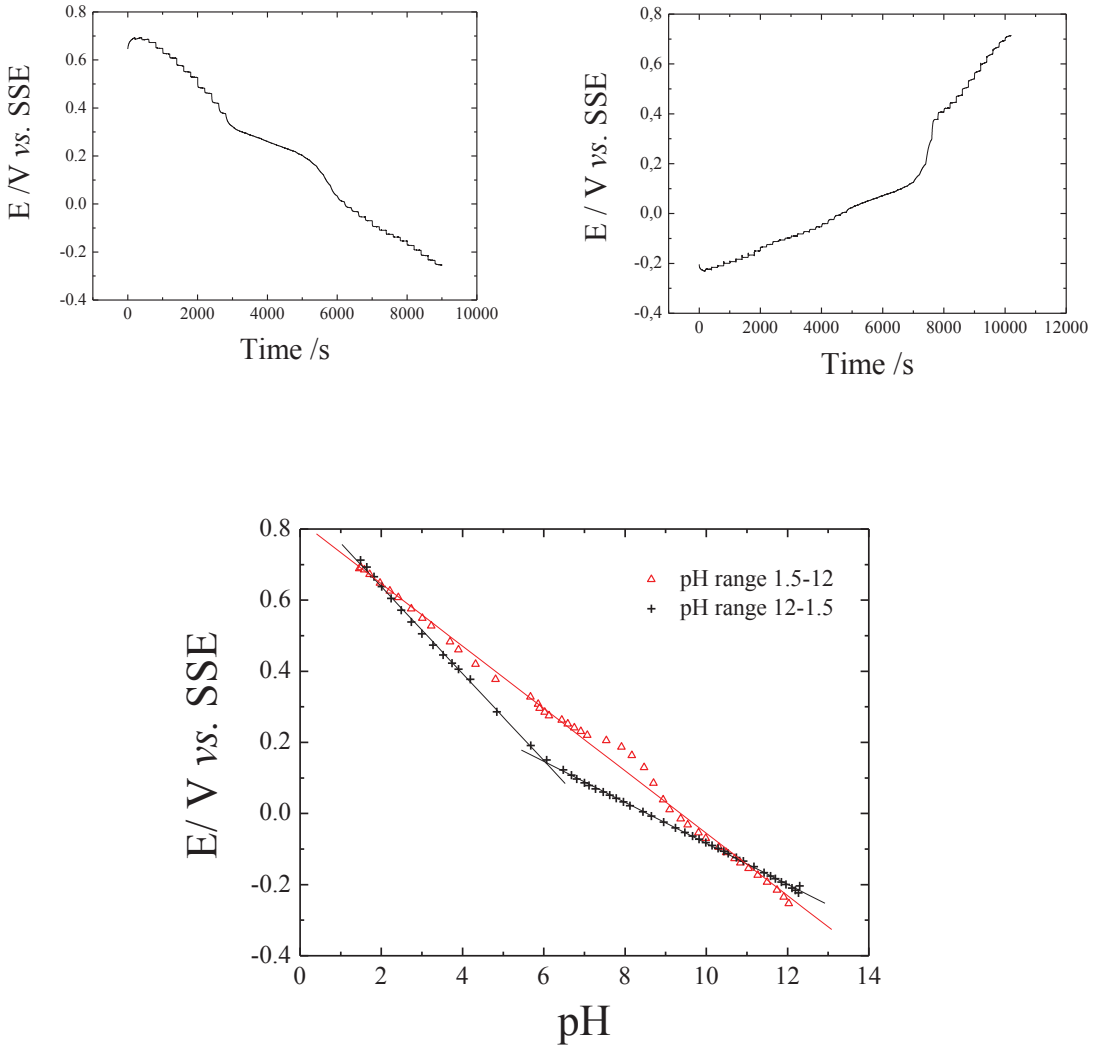

Figure 8: Potentiometric response as a function of time, of an electrode resulting from the electrodeposition of a MnO_2 thin film on a glassy carbon electrode: open circuit potential plotted as a function of a, b) time, c) pH. The investigated pH range was described as follows: 1) trace (titration of an aqueous H_2SO_4 solution with an aqueous NaOH from pH 1.5 to 12), 2) re-trace (titration of the resulting solution with an aqueous H_2SO_4 solution from pH 12 to 1.5).

Figure(s)

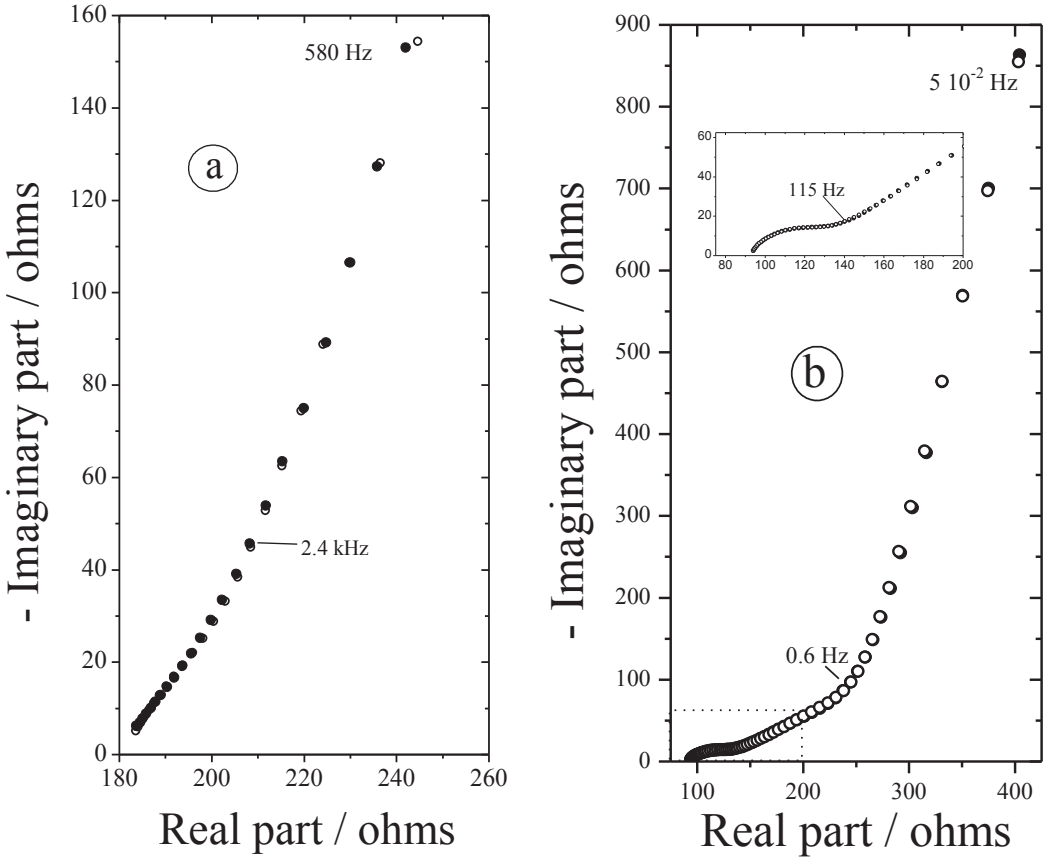

Figure 9: EIS spectra obtained at a) a bare GC electrode, b) a MnO_2 coated GC electrode, at open circuit potential in an aqueous H_2SO_4 solution (pH = 1.8). Ref = SSE. CE = Pt.
(○) Fitted values ; (●) experimental values.

Figure(s)

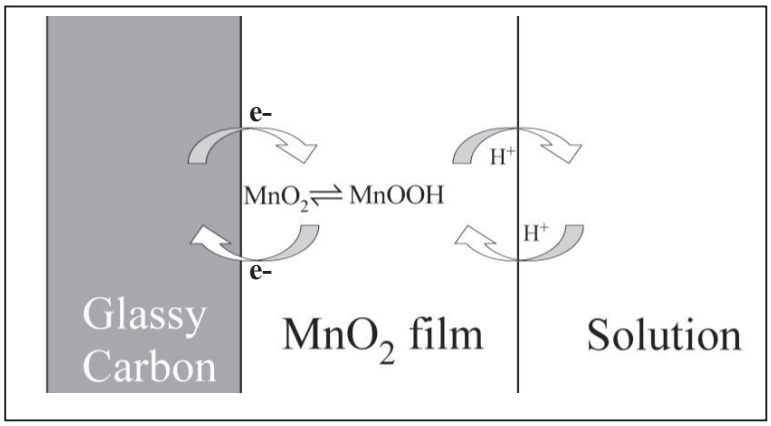

Figure 10: Scheme of the oxide film coated GC electrode used as pH sensor.

Figure(s)

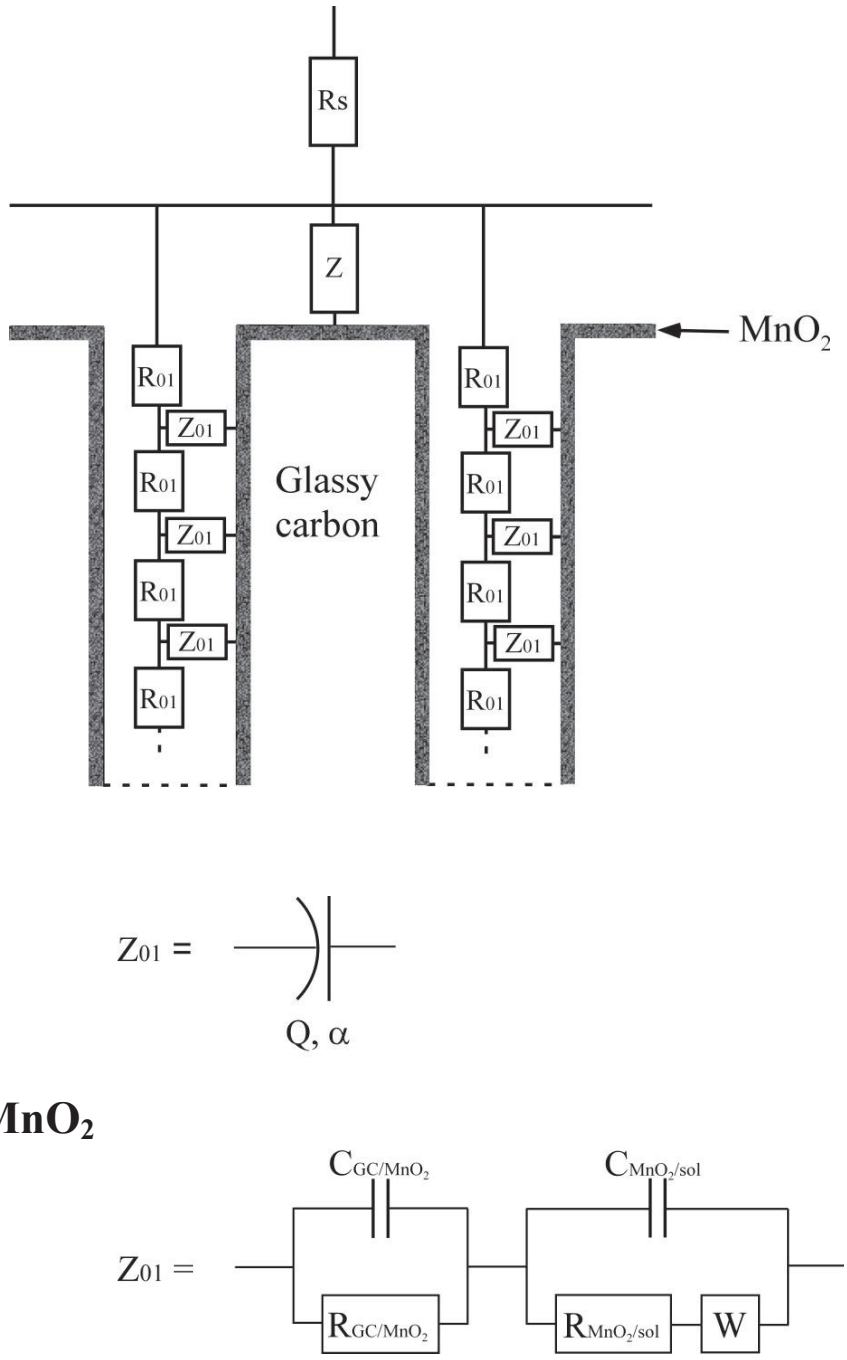

Figure 11: a) Model and equivalent circuit of a porous electrode with non adjoining pores, b) Z_{01} impedance for the GC electrode, c) Z_{01} impedance for the GC/MnO_2 electrode.